科技部補助

大專學生研究計畫研究成果報告

計 畫

A noise characterization and analysis method

based on Bloch sphere dynamics

名 稱

報告類別:成果報告執行計畫學生:施麗釵

學生計畫編號: MOST 110-2813-C-002-038-M

研 究 期 間 : 110年07月01日至111年02月28日止,計8個月

指 導 教 授 : 鄭原忠

處 理 方 式 : 本計畫可公開查詢

執 行 單 位 : 國立臺灣大學化學系暨研究所

中 華 民 國 111年03月30日

摘要

目前的量子電腦被稱為雜訊中等規模量子電腦(NISQ 電腦),發展受到雜訊影響而受限,只能進行小規模計算且無法達成預期的應用。為了實現量子電腦的實際應用,了解雜訊至關重要,分析雜訊有助於保護量子資訊受到影響和 NISQ 電腦的開發。目前測量錯誤率的主要方法是隨機基準測試(RB)。 RB 方法將來自不同量子邏輯閘的雜訊視為相同的雜訊,然而若不同的量子邏輯閘具有不同類型的雜訊,這種測量錯誤率方法就會有很多的討論空間。

在這項研究中,藉由定量和定性的去分析 IBM-Q 系統中的雜訊,我們開發了一種能識別量子邏輯閘與環境中雜訊的方法。我們藉由恆等閘引入雜訊,將實驗結果畫在布洛赫球體上,並且藉由量子主方程去擬合球體上軌跡的動力學,來得到實驗中雜訊動態的變化,也就是說,我們可以提取實驗過程中的雜訊,利用初始值便可重現原本的軌跡,並且針對其性質進行分析。了解量子電腦上詳細的雜訊性質有助於模擬開放量子系統動力學中的量子雜訊。利用特殊序列的量子邏輯閘引進特定形式的雜訊,我們模擬了在開放式量子系統下簡單的能量轉移模型。詳細了解IBM-Q 量子電腦上單一量子位元系統的雜訊,對於未來應用在量子電腦上的錯誤修正演算法或錯誤緩解演算法至關重要,將有助於現階段量子電腦的發展。

Abstract

Quantum simulations of chemical systems remain the most promising target applications of near-term quantum computers. Yet, the small size and significant noise levels of quantum computers nowadays critically hamper the practicality of the applications. Current quantum devices are termed noisy intermediate-scale quantum devices (NISQ devices), which can only do small-scale calculations. Analysis of noises can be beneficial for protecting quantum information from errors and the development of NISQ devices. It is critical to understand noises in order to achieve the real-world application of quantum computers. The primary method of error rate measurement nowadays is randomized benchmarking (RB). The RB method views all noises from different gates as the same; however, various quantum gates have different types of noises, which is worth discussing.

In this research, we develop a method to quantitatively identify the noises of quantum gates and systematically analyze noises in the IBM-Q systems. By fitting the Bloch sphere dynamics with the quantum master equation, we can obtain information about noises in the experiment. In other words, we can extract the noise information in the experiment. The detailed noises characterization on quantum computers can be beneficial for simulating the quantum noises in open quantum system dynamics, which

can be a significant application of NISQ devices. Understanding the detailed mechanism of the underlying noises about IBM-Q quantum computers is vital for error mitigation protocols for the future of the quantum computer.

Contents

摘要	i
Abstract	ii
Contents	iv
1 Background	1
1.1 Noise-prone quantum computer	1
1.2 Randomized benchmarking method	2
1.3 Domestic development of quantum computer	3
1.4 Motivation	4
2 Introduction to Quantum Computing	6
2.1 Quantum bits (Qubit)	6
2.2 Density matrix	7
2.3 Quantum gate and measurement	9
2.4 Open quantum system	11
2.5 Quantum master equations and markovian assumption	12
2.6 Noise distribution	14
3 Methodology	15

	3.1 Characterization of noise-introducing identity gate	15
	3.2 Quantum state tomography	16
	3.3 Noise information extraction by numerical analysis method	18
	3.3 The Forward Euler method	19
	3.4 The Crank-Nicolson method	20
	3.5 The Outline of this work	21
	4 Results and Discussion	23
	4.1 Characterization for Pauli gates in one qubit system	23
	4.2 Noise decomposition and simulation of (X) ² gates	27
	4.3 Correlation error in a two-qubit system	29
	4.4 Compensating pulse sequence design –(XZXZZ) ² gates	30
:	5 Conclusion	32
(6 References	34
,	7 Appendix	36
	Appendix A. Mathematical details in the Forward Euler method	36
	Appendix B. Application details in the Crank-Nicolson method	38
	Appendix C. Variance of the depolarizing rate of $(XZXZZ)^2$ and $(X)^2$	40
	·	

1 Background

1.1 Noise-prone quantum computer

Quantum computers harness the intrinsic properties of quantum mechanics, which offer the promise of efficiently solving specific problems that are intractable for classical computers. 1-3 Quantum computers are believed to solve some computational issues that are hard for classical computers, such as integer factorization² (which underlies RSA encryption⁴), cryptography, search problems, machine learning⁵, and simulation of quantum chemical systems⁶. Quantum computers rely on qubits to store information. However, qubits are fragile that their stored quantum information can be scrambled easily. In addition, the preparation and the measurement of the quantum state could cause noise. Noises make quantum computers error-prone, and they are the central obstacles to building large-scale quantum computers and make computing results unreliable. Under current restrictions, simulation of chemical systems is a focus of NISQ devices. 7 (Figure 1.1)

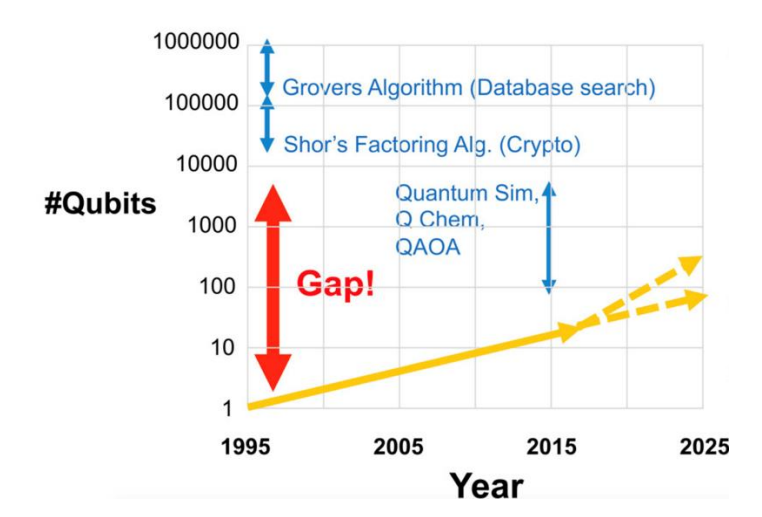


Figure 1.1 The gap between quantum algorithms and machines. Quantum simulation of chemical systems is the most promising target application of near-term quantum computers. The figure is taken from https://arxiv.org/abs/1903.10541

1.2 Randomized benchmarking method

The road to developing and operating devices that would enable quantum computation has been and continues to be full of obstacles. One of the main challenges in building a quantum information processor is the non-scalability of completely characterizing the noise affecting a quantum system. When we got the information in the system through measurement, the noise from state preparation and measurement (SPAM errors) that affected qubits would be toke into account. To easily determine the current system's performance, randomized benchmarking (RB), a scalable and robust algorithm for benchmarking the full set of Clifford gates by a single parameter using randomization techniques, is applied to characterize the noise.⁸

To benchmark the noise of gates, the RB sequences are randomly chosen in Clifford

elements and the reversal element, which can make the overall transformation be the identity. (Figure 1.2) After executing the RB sequences, we measure the system and get the averaged sequence fidelity for calculating the average error-rate related to the RB sequences' average performance. The RB method is widely used in many companies, such as IBM and Google, for its scalability and robustness.

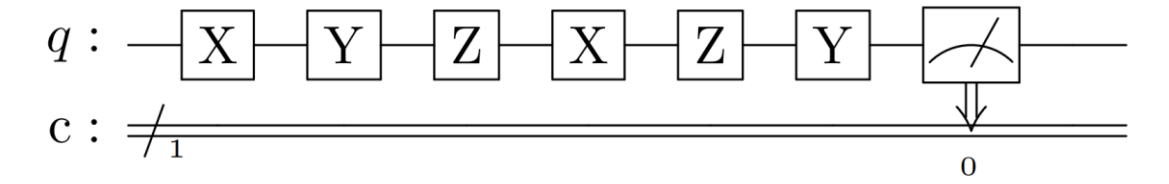


Figure 1.2 Example of the RB sequences. The characters in the blocks present different quantum gates. We need to notice that twice the Pauli gates (Pauli X, Pauli Y, and Pauli Z) equals the identity gate, which means that the qubit would be the initial state after applying these RB sequences.

1.3 Domestic development of quantum computer

Taiwan proposed the concept of establishing a national quantum team by interministerial associations. By 2026, 8 billion dollars will be invested to promote the country's technology and talent in this field, and it is finally officially launched. To develop our quantum computer, scientists contributed many efforts. Taiwan recently focused on building qubits, which is the base of the quantum computer. The qubit amount that has been made is about 1-2. There are many types of quantum computers, including

superconducting quantum computers, ion-trapped quantum computers, and semiconducting quantum computers. No matter which types the quantum computer is, how to characterize the quantum system and how to calibrate the quantum system is a matter of concern. An algorithm that focuses on characterizing a basic one-qubit system will be helpful in this current stage.

1.4 Motivation

In the RB method, we consider the average performance of the RB sequences to identify the error rate of gates; however, we consider that different gates may have different kinds of noises. If we average their performance, we may underestimate the error rate, which can be troublesome when we use some quantum algorithms that majorly use specific gates. In a nutshell, quantum computers are developing technologies while the main obstacles are noises. The primary method of noise characterization is too simplified to analyze the noise. To have a more profound understanding of the behavior of each quantum gate, we want to establish a method to characterize the basic noise on the quantum computer, including an analysis of the noise of quantum gates and the environment.

This research aims to develop a method to analyze noise composition for each

possible quantum gate, decompose the noise into specific simple noise channels, and design gate sequences to mitigate or transform certain types of quantum noise. Furthermore, we intend to fully characterize the noises of one qubit system on the IBM-Q quantum computer in **Table 1**. The algorithm emphasizes the characterization of quantum errors based on a dynamical map approach which can be easily imagined over a quantum dynamic. We expect our study can obtain a better understanding of quantum noises. It can be beneficial for noise characterization and quantum error correction.

What is more, it can assist the development of quantum computers, including the simulation of chemical systems. Analysis of noises can be beneficial for protecting quantum information from errors and the development of NISQ devices. It is critical to understand noises in order to achieve the real-world application of quantum computers.

Machine Name	Qubits	Quantum Volume
Paris	27	32
Bogota	5	32
Manhattan	65	32

Table 1. IBM-Q machine examined in this research.

2 Introduction to Quantum Computing

The following section will discuss the basic concept and math, including quantum bits, density matrix, and Bloch Sphere. Besides, we will also present some theoretical background, including the open quantum system, markovian process, and Gaussian distribution.

2.1 Quantum bits (Qubit)

In classic computers, a bit can be in the state 0 or 1. By contrast, a qubit can exist in a quantum computer in a continuum of states between $|0\rangle$ and $|1\rangle$. Until we observe the qubit, it will be in its superposition state:

$$|\psi\rangle = \alpha|0\rangle + \beta|1\rangle,\tag{2.1.1}$$

where α and β are complex numbers, called probability amplitude.

When we measure a qubit, we obtain either the result 0, with a probability $|\alpha|^2$, or the result 1, with probability $|\beta|^2$. Naturally, $|\alpha|^2 + |\beta|^2 = 1$, since the probabilities must sum to one. While the general state of one qubit is

$$|\psi\rangle = \cos\frac{\theta}{2}|0\rangle + e^{i\varphi}\sin\frac{\theta}{2}|1\rangle,$$
 (2.1.2)

where θ and ϕ are real numbers, θ ranges from 0 to π , and ϕ ranges from 0 to 2π . We can also write the quantum state in a vector notation as

$$|\psi\rangle = \begin{pmatrix} \cos\frac{\theta}{2} \\ e^{i\varphi}\sin\frac{\theta}{2} \end{pmatrix}. \tag{2.1.3}$$

The numbers θ and φ define a point on the unit three-dimensional unit-sphere, the Bloch sphere, which provides a useful way of visualizing a single qubit's state. (**Figure 2.1**) Here we denote the four specific quantum states that are on the point of the X-axis, Y-axis, and Z-axis:

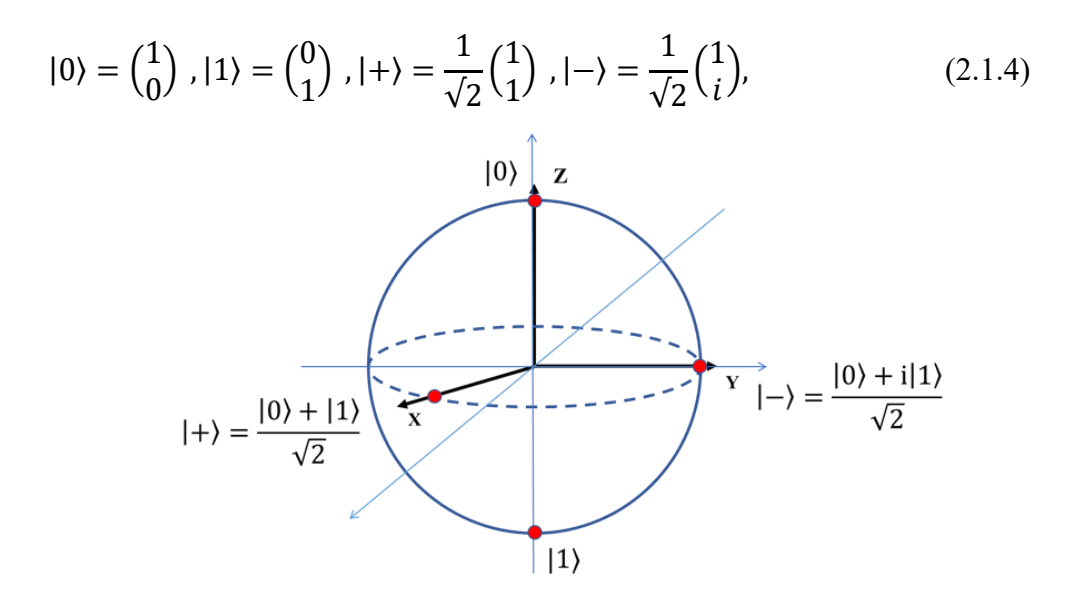


Figure 2.1 Bloch sphere representation of a qubit state. The four points stand for four specific quantum states mentioned in equation (2.1.4).

2.2 Density matrix

The state vectors in equation (2.1.3) define the pure quantum states. When the quantum state is mixed, we can adopt a density matrix⁹ or density operator to describe the quantum system and its evolution. The evolution of a closed quantum system can be described by the unitary operator U. If the system was initially in the state $|\psi_i\rangle$ with probability p_i

then after the evolution has occurred, the system will be in the state $U|\psi_i\rangle$ with probability p_i . With the definition of the density matrix, the evolution of the system can be described by

$$\rho \equiv \sum_{i} p_{i} |\psi_{i}\rangle\langle\psi_{i}| \stackrel{U}{\to} \sum_{i} p_{i} U |\psi_{i}\rangle\langle\psi_{i}| U^{\dagger} = U \rho U^{\dagger}. \tag{2.2.1}$$

For one qubit system, the density matrix would be a 4×4 matrix, and its basis can be Pauli matrices σ_i (i = X, Y, Z, I), which are Hermitian and unitary.

$$X = \sigma_{x} = \begin{pmatrix} 0 & 1 \\ 1 & 0 \end{pmatrix}, X^{\dagger} = X,$$

$$Y = \sigma_{y} = \begin{pmatrix} 0 & -i \\ i & 0 \end{pmatrix}, Y^{\dagger} = Y,$$

$$Z = \sigma_{z} = \begin{pmatrix} 1 & 0 \\ 0 & -1 \end{pmatrix}, Z^{\dagger} = Z,$$

$$I = \sigma_{I} = \begin{pmatrix} 1 & 0 \\ 0 & 1 \end{pmatrix}, I^{\dagger} = I,$$

$$(2.2.2)$$

where different matrices can represent different gates. (Identity gate means doing nothing) For one qubit system, the pure density matrix can be expanded by its bases, the Pauli matrices:

$$\rho = \frac{I + r_x X + r_y Y + r_z Z}{2}.$$
 (2.2.3)

The density matrix can be drawn on the Bloch sphere with the vector $\vec{v} = (r_x, r_y, r_z)$ where r_i corresponds to the projection length of the Bloch vector on the i-axis. We can know the density matrices of mentioned quantum states in equation (2.2.4) by equation (2.2.5):

$$|0\rangle\langle 0| = \begin{pmatrix} 1 & 0 \\ 0 & 0 \end{pmatrix} = \frac{1}{2}(I+Z), \vec{v} = (0,0,1)$$

$$|1\rangle\langle 1| = \begin{pmatrix} 0 & 0 \\ 0 & 1 \end{pmatrix} = \frac{1}{2}(I-Z), \vec{v} = (0,0,-1)$$

$$|+\rangle\langle +| = \frac{1}{\sqrt{2}}\begin{pmatrix} 1 & 1 \\ 1 & 1 \end{pmatrix} = \frac{1}{\sqrt{2}}(I+X), \vec{v} = (1,0,0)$$

$$|-\rangle\langle -| = \frac{1}{\sqrt{2}}\begin{pmatrix} 1 & -i \\ i & 1 \end{pmatrix} = \frac{1}{\sqrt{2}}(I+Y), \vec{v} = (0,1,0).$$
(2.2.4)

We can notice that the Pauli matrix shown in four specific states is related to what axis the state is on.

2.3 Quantum gate and measurement

When applying the operation on the qubit, we can write the operation into the mathematical form and visualize the operation by the Bloch sphere. With the density matrix of the initial state and the different operators with equation (2.2.2), we can map the density matrix to the Bloch sphere to see how the operators behave. Application of different gates means rotating the vector (quantum state) 180 degrees around the different axis on the Bloch sphere. (**Figure 2.2**) Applying the same Pauli gate twice to the same qubit can cancel out the operation, which brings us to the following identity:

$$X^2 = Y^2 = Z^2 = I. (2.2.5)$$

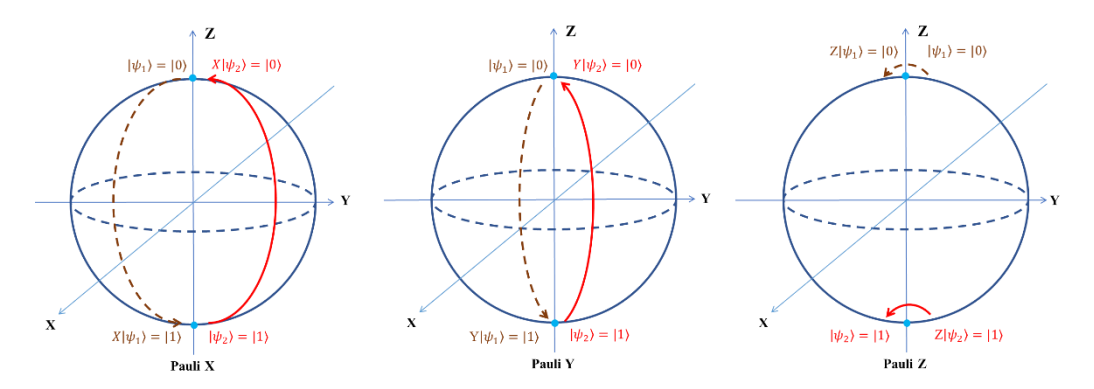


Figure 2.2 Different gates shown on the Bloch sphere.

Quantum operations or quantum gates are performed by sending electromagnetic impulses at microwave frequencies to the resonator coupled to the qubit. (**Figure 2.3**) This frequency resonates with the energy separation between the energy levels for $|0\rangle$ and $|1\rangle$. As for the measurement, it sends a microwave tone to the resonator and analyzes the signal it reflects back. The amplitude and phase of the reflected signal depend on the qubit state. By default, all qubits are initialized in the $|0\rangle$ state in the z-basis. Therefore, qubit measurement is generally in a z-basis.

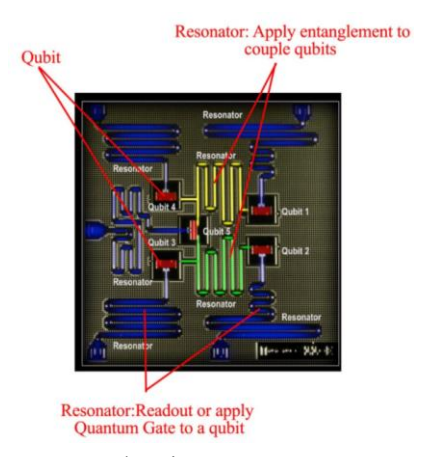


Figure 2.3 IBMQ 5 qubits superconducting quantum computer. Figure is taken from https://jonathan-hui.medium.com/qc-how-to-build-a-quantum-computer-with-superconducting-circuit-4c30b1b296cd

With the interference of the noises, the operator (gate) could have the error that can display on the Bloch sphere dynamic. For instance, after the ground state $|0\rangle$ is applied the $(X)^2$ gates, the point on the Bloch sphere should stay on the intersection at the sphere surface and the positive z-axis if the X gate is perfect. The noises make the points a trajectory on the Bloch sphere. The different noises make the different tendencies of the behavior of the trajectory. The noise characterization method is major based on Bloch sphere dynamics in this research.

2.4 Open quantum system

We can view a quantum computer as a device that can simulate a quantum system. When the quantum computer is still suffering the noises from the environment, we have to consider the problem as an open quantum system. The open quantum system¹¹ means that the system we care for interacts with an external quantum system (bath or environment). If the quantum system is in a closed quantum system, it will retain its coherence. Still, the interaction between the quantum system and the external quantum system will happen when we try to control or measure the system. When the system interacts with the environment, the information might flow or be lost from the system to the environment, called decoherence. Decoherence errors from the environment affect the

qubit state and make the qubit fragile. The schematic picture has shown in **Figure 2.4**, where the red pulse represents the operations.

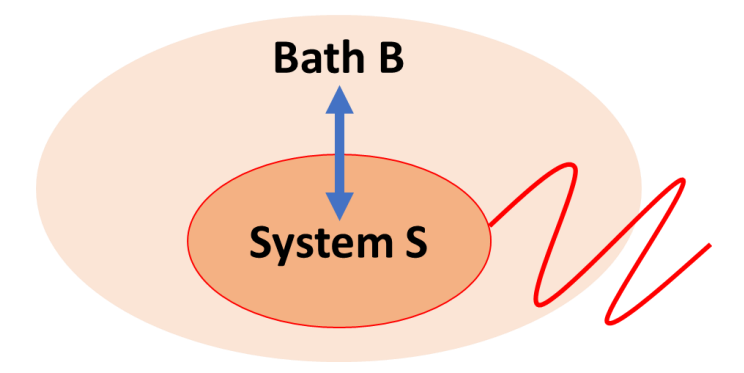


Figure 2.4 Schematic picture of an open quantum system.

2.5 Quantum master equations and markovian assumption

To describe the open quantum system dynamics, we can use the quantum master equation 10 , where the master equation is a differential equation that corresponds to the time evolution. This research views the trajectory result of measurement in a noisy environment as a stochastic process. If we assume that the process is markovian 11 , instead of the past state and the present state, we only need the present state to know the future states of the trajectory. In other words, we assume that the correlation time δt_B that the bath needs to lose the information flow from the system forever is very short, and we can ignore the memory effect of the bath. If we denote δt_S as the time takes for the dynamics we want to observe; the relationship would be:

$$\delta t_S \gg \delta t_B.$$
 (2.5.1)

In this assumption, we use the stochastic Liouville equation 12-13 to describe the system:

$$\frac{d\rho(t)}{dt} = -\frac{i}{\hbar}[H(t), \rho(t)] + p\sum_{i} \left(L_{i}\rho(t)L_{i}^{\dagger} - \frac{1}{2}\left\{L_{i}^{\dagger}L_{i}\rho(t)\right\}\right),\tag{2.5.2}$$

where H is noise Hamiltonian, which is caused by the imperfect gates, p is the error rate and L_i corresponds to noise operator. The first term of the right-hand side of equation (2.5.2) can be interpreted as the unitary evolution (the length of the Bloch vector keeps the same) because of the gate error. And the second term can be interpreted as systembath coupling. We can choose the proper noise channel to describe the trajectory, and the quantum operations of the noise channel determine the noise operators⁹.

Nowadays, several known operation elements exist for important single qubit quantum operations, such as depolarizing channel, amplitude damping, and phase damping. In Table 2, we show the detailed operation elements, where p and γ are the error rates.

depolarizing channel	$E_{1} = \sqrt{1 - \frac{3p}{4} \begin{bmatrix} 1 & 0 \\ 0 & 1 \end{bmatrix}}, E_{2} = \sqrt{\frac{p}{4}} \begin{bmatrix} 0 & 1 \\ 1 & 0 \end{bmatrix},$ $E_{3} = \sqrt{\frac{p}{4}} \begin{bmatrix} 0 & i \\ -i & 0 \end{bmatrix}, E_{4} = \sqrt{\frac{p}{4}} \begin{bmatrix} 1 & 0 \\ 0 & -1 \end{bmatrix}$	
amplitude damping	$E_1 = \begin{bmatrix} 1 & 1 \\ 0 & \sqrt{1-\gamma} \end{bmatrix}, E_2 = \begin{bmatrix} 0 & \sqrt{\gamma} \\ 0 & 0 \end{bmatrix}$	
phase damping	$E_1 = \begin{bmatrix} 1 & 1 \\ 0 & \sqrt{1-\gamma} \end{bmatrix}, E_2 \begin{bmatrix} 0 & 0 \\ 0 & \sqrt{\gamma} \end{bmatrix}$	

Table 2. Operation elements for important single qubit quantum operations.

2.6 Noise distribution

When processing the noise problem, we often assume that the distribution of the noises is Gaussian distribution (normal distribution). According to the Central Limit Theorem (CLT)¹⁴, the distribution of a set of random variables would be a Gaussian distribution. The approximation in this theorem is that the sample size is sufficiently large and random enough. If the distribution is non-Gaussian, we can figure out how non-Gaussian it is and the possible reasons, such as extreme values, insufficient data size, or natural limit of hardware. It is important to characterize the noise with these statistical properties.

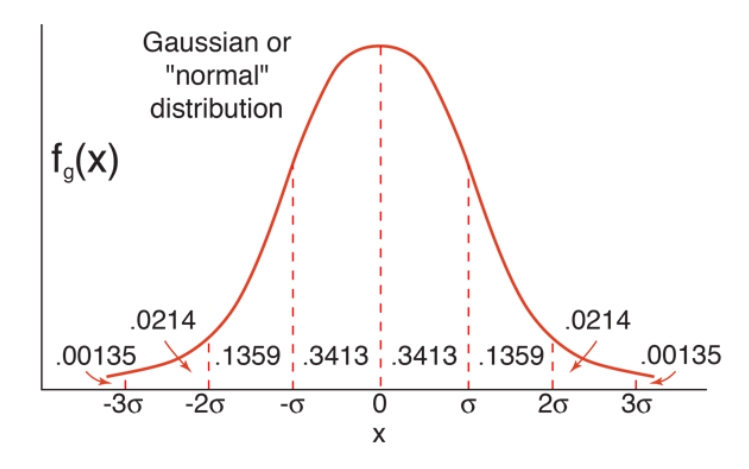


Figure 2.5 Gaussian distribution function. The probability of finding the value is related to which interval of the standard deviation of the mean the value is within. Figure is taken from https://jonathan-hui.medium.com/qc-how-to-build-a-quantum-computer-with-superconducting-circuit-4c30b1b296cd

3 Methodology

In this study, we aim to observe gate errors by using the identity gate (composed of multiple Pauli gates) and focus on the one qubit system first for basic noise characterization

3.1 Characterization of noise-introducing identity gate

As shown in the equation (2.2.5) and **Figure 2.2**, applying the same Pauli gate twice to the same qubit should be the same as applying an identity gate. Because the qubit measurement is generally in z-basis and the Y gate can be decomposed to X gate and virtual Z gate:

$$Y = i XZ. (3.1.1)$$

We choose the X gate as our primary object of observation and take the four specific states mentioned in equation (2.2.4) as the initial states. We can obtain the population by dividing the number of 0 or 1 when the initial state is $|0\rangle$ or $|1\rangle$ by measurement times.

We run the circuit on an IBM-Q quantum computer to see the performance of the $(X)^2$ gates. (Figure 3.1)

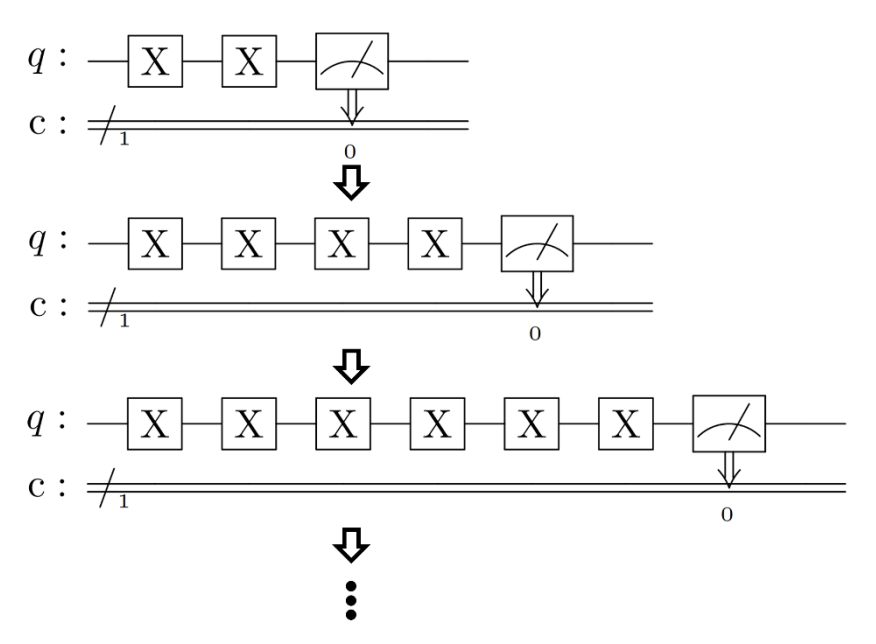


Figure 3.1 Schematic picture of the circuit. The number of $(X)^2$ gates are increased to see the dynamics of the noises. The state preparation operations have not been shown in this figure.

To prepare the different initial states, we need to apply different gates. All qubits are initialized in the $|0\rangle$ state:

$$|1\rangle = X|0\rangle = \begin{pmatrix} 0 & 1\\ 1 & 0 \end{pmatrix} \begin{pmatrix} 1\\ 0 \end{pmatrix} = \begin{pmatrix} 0\\ 1 \end{pmatrix}, \tag{3.1.2}$$

$$|+\rangle = H|0\rangle = \frac{1}{\sqrt{2}} \begin{pmatrix} 1 & 1 \\ 1 & -1 \end{pmatrix} \begin{pmatrix} 1 \\ 0 \end{pmatrix} = \frac{1}{\sqrt{2}} \begin{pmatrix} 1 \\ 1 \end{pmatrix},$$
 (3.1.3)

$$|-\rangle = SH|0\rangle = \frac{1}{\sqrt{2}} \begin{pmatrix} 1 & 0 \\ 0 & i \end{pmatrix} \begin{pmatrix} 1 \\ 0 \end{pmatrix} = \frac{1}{\sqrt{2}} \begin{pmatrix} 1 \\ i \end{pmatrix}.$$
 (3.1.4)

3.2 Quantum state tomography

Apart from the population, we obtain the density matrix by quantum state tomography and see the Bloch sphere dynamics. Quantum state tomography⁹ is a method for determining the quantum state of a system. Since the quantum state can't be directly

determined by measurement, we need to perform repeated preparations of the same quantum state, which is then measured in different ways in order to build up a complete description of the quantum state. From equation (2.2.5), we know the definition of the density matrix, which can completely express the quantum state. Suppose we have many copies of a single qubit density matrix, ρ . The set $\frac{I}{\sqrt{2}}$, $\frac{X}{\sqrt{2}}$, $\frac{Y}{\sqrt{2}}$, $\frac{Z}{\sqrt{2}}$ forms an orthonormal set of matrices concerning the Hilbert–Schmidt inner product, so ρ may be expanded as

$$\rho = \frac{tr(\rho)I + tr(\rho X)X + tr(\rho Y)Y + tr(\rho Z)Z}{2},$$
(3.2.1)

where $tr(\rho A)$ equals the average value of observables. The measurement result would be 0 or 1. We can calculate the observables by the number of measurements (in Z basis):

$$tr(\rho Z) = \frac{(number\ of\ 0) * 1 + (number\ of\ 1) * -1}{number\ of\ measurements}.$$
 (3.2.2)

We map the density matrix to the Bloch sphere to obtain further observation. The average value of observables can form a state vector on the Bloch sphere:

$$\vec{v} = (tr(\rho X), tr(\rho Y), tr(\rho Z)) = (r_x, r_y, r_z). \tag{3.2.3}$$

And the length of the state vector is proportional to the purity:

$$\gamma \equiv \operatorname{tr}(\rho^2). \tag{3.2.4}$$

With state tomography, we can obtain the density matrix and the Bloch sphere and construct the Bloch sphere dynamics by gaining the density matrix each time after the increasing number of $(X)^2$ gates. On the other hand, with the known density matrix of

initial states mentioned in equation (2.2.8), the density matrix after applying the operator can be expressed as

$$\mathcal{E}(\rho) = \sum_{k} E_{k} \rho E_{k}^{\dagger}, \tag{3.2.5}$$

where E_k are operation elements, satisfying $E_k^{\dagger}E_k=I$ if the quantum operation is trace-preserving.

3.3 Noise information extraction by numerical analysis method

This research aims to extract the noise information in the Bloch sphere dynamics by numerically analyzing the open system dynamics. By measurement, we can know the density matrix of each step while the Hamiltonian and the error rate of the noise are unknown to us. We can use the quantum master equation mentioned in equation (2.5.2) to describe the open quantum dynamics. We can find the Hamiltonian by considering whether the evaluated density matrix of the state is close to the experimental result. In other words, the trace distance of the two matrices should be minimized.

$$T(\rho, \rho_{theory}) = \frac{\left| \left| \rho(t_{n+1}) - \rho_{theory}(t_{n+1}) \right| \right|}{2}, \tag{3.2.5}$$

where ρ is the density matrix obtained in the experiment and ρ_{theory} is the theoretically evaluated density matrix. If T (ρ , ρ_{theory}) = 0, meaning that the Hamiltonian and the error rate have correctly described the open quantum system.

We can use numerical methods to propagate the system with the optimized condition.

The numerical methods we used in this research are the Forward Euler method and the Crank-Nicolson method.

3.3 The Forward Euler method

The Forward Euler method¹⁵ is a simple method to process the differential equation

$$\frac{dy}{dt} = f(t, y),\tag{3.3.1}$$

which is the form of the quantum master equation we care about. By the Taylor expansion and truncating the equation at the second-order term, we can rewrite the equation as

$$y(t_{n+1}) = y(t_n) + (t_{n+1} - t_n)y'(t_n). (3.3.2)$$

By defining $\Delta t = t_{n+1} - t_n$, we can get the equation

$$\frac{y(t+\Delta t)-y(t)}{\Delta t}=f(t,y(t)), \tag{3.3.3}$$

where y(t) corresponds to the density matrix we get in the experiment, and f(t, y(t)) includes the information of noise Hamiltonian and the error rate.

To check whether the operator in f(t, y(t)) is unitary, we apply the equation to the Time-Dependent Schrödinger Equation (we set $\hbar = 1$):

$$\frac{\Psi(t+\Delta t)-\Psi(t)}{\Delta t}=-iH\Psi(t). \tag{3.3.4}$$

By reorganizing the equation, the propagator in this equation is

$$U(0, \Delta t) = 1 - iH\Delta t. \tag{3.3.5}$$

And we know that

$$UU^{\dagger} = (1 - iH\Delta t)(1 + iH\Delta t) \neq I. \tag{3.3.6}$$

Therefore, we know that the Forward Euler method is a first-order explicit numerical method and its propagation method is non-unitary.

There is another method called the Backward Euler method, which like the Forward Euler method, is a first-order implicit method.

$$\frac{y(t+\Delta t)-y(t)}{\Delta t}=f(t+\Delta t,y(t+\Delta t)), \tag{3.3.7}$$

The local truncation error of the Euler method is approximately proportional to $(\Delta t)^2$ and the global error is approximately proportional to Δt . The large truncation error will be a significant problem in long-time propagation.

The mathematical detail of the Forward Euler method in this research has been attached in Appendix A.

3.4 The Crank-Nicolson method

We use the Crank-Nicolson method¹⁵ to avoid the large truncation error from the Forward Euler method. The Crank-Nicolson method considers the Forward Euler method and backward Euler method simultaneously. The equation is

$$\frac{y(t + \Delta t) - y(t)}{\Delta t} = \frac{1}{2} (f(t, y(t)) + f(t + \Delta t, y(t + \Delta t))), \tag{3.4.1}$$

which is both implicit and explicit. To check whether the propagation is unitary, similarly, we apply the equation to the Time-Dependent Schrödinger Equation and get

$$\frac{\Psi(t+\Delta t) - \Psi(t)}{\Delta t} = -\frac{i}{2} \Big(\widehat{H} \Psi(t) + \widehat{H} \Psi(t+\Delta t) \Big). \tag{3.4.2}$$

By reorganizing the equation, the propagator in this equation is

$$U(0, \Delta t) = (1 + \frac{iH\Delta t}{2})^{-1} (1 - \frac{iH\Delta t}{2}). \tag{3.4.3}$$

And we can know that

$$UU^{\dagger} = I. \tag{3.4.4}$$

This method can process the problem by considering the noise Hamiltonian as the coherence part from the imperfect gate and the error rate as the decoherence part from the environment.

The application details of the Crank-Nicolson method in this research has been attached in Appendix B.

3.5 The Outline of this work

To sum up, everything that has been stated so far: firstly, we start from the $(X)^2$ gates, the identity gate. We observe the change in the fidelity of the population when the number of $(X)^2$ gates are increasing. Secondly, to further understand the effect of the

coherence and the decoherence noises, we perform quantum state tomography to obtain density matrices and observe the purity change during the process. Next, we draw the Bloch sphere dynamic to look into the major noises of the quantum gate. We utilize the known noise channel and the quantum master equation to decompose the noise and obtain the error rates and noise Hamiltonian in each experiment step. After fitting the experimental result, we can reproduce the Bloch sphere dynamic by the noise channel and the noise Hamiltonian with the initial condition. Finally, we can extract the information about noise in the experiment and analyze the noise dynamics during the experiment and the overall noise information.

4 Results and Discussion

4.1 Characterization for Pauli gates in one qubit system

As a first step to understanding the qubit dynamics induced by (X)² gates, we initialized a single qubit in the ground state and applied (X)² gates multiple times. After the (X)² gates, projective measurement in a computational basis is performed to calculate the population remaining in the ground state. We plotted the ground state populations as a function of the number of $(X)^2$ gates (Figure 4.1). The results are grouped according to (a) different times and (b) different physical qubits. In both cases, the ground state populations significantly decrease, and the dynamics behave as highlynoisy oscillations. The population then finally reach equilibrium around 0.5 at >1000 (X)² gates. We speculated that two predominating types of error in the X gates could explain the dynamics. An over-rotation of the X gates results in the population inversion at the initial stages. Decoherent-type error dominates at many X gates, which drives the population towards equilibrium. We thus perform further state characterization to assess the dynamics of the noises induced by $(X)^2$ gates. Furthermore, the population dynamics under different parameters behave very differently, even qualitatively, which also signifies the highly unstable nature of the gate noises.

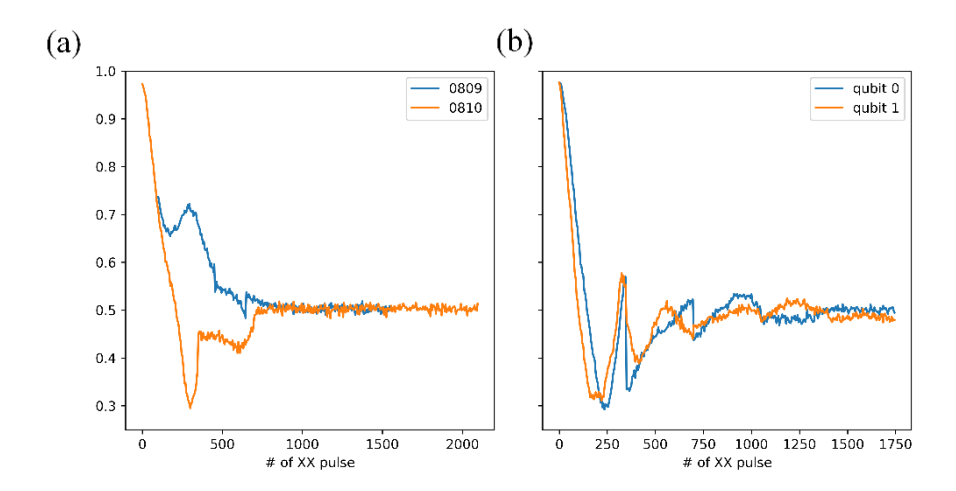


Figure 4.1 Single qubit population dynamics for the $(X)^2$ gates. Ground state populations as functions of the number of applied X^2 gates are plotted. In (a), the experiments were performed on different days (8/9 and 8/10) but same physical qubit. In (b), the two experiments are performed on different physical qubits. All experiments were performed on ibmq_ourense.

The purity changes of the four initial states are shown in **Figure 4.2.** When the initial state is $|+\rangle$, the change of purity shows special stability. Hence, we turn to see the Bloch sphere dynamics to achieve further (**Figure 4.3**). Finding that the huge amount of $(X)^2$ gates caused the vector of the density matrix to move around the axis of X, and the length of the vector decreased with the increasing number of $(X)^2$ gates. When the initial state is $|+\rangle$, the vector on the Bloch sphere is right on the X-axis, the influence of rotation from $(X)^2$ gates would be smaller. We find that $(X)^2$ gates cause similar noise, which makes the vector on the Bloch sphere rotate and be shorter. Consequently, we analyze the composition of noise described by the depolarizing noise channel and Rx form. We replace $(X)^2$ gates with R_X and consider the depolarizing channel by using operator-

sum representation. Besides, we also see the Bloch sphere dynamics of $(Z)^2$ gates (Figure 4.4). We find that no matter how much $(Z)^2$ gates we apply, the vector of the density matrix stays on its initial position, which means that the gate error of the Z gate is near zero. It is appreciable because the Z gate on IBM-Q quantum computers can be implemented virtually in hardware via frame changes.

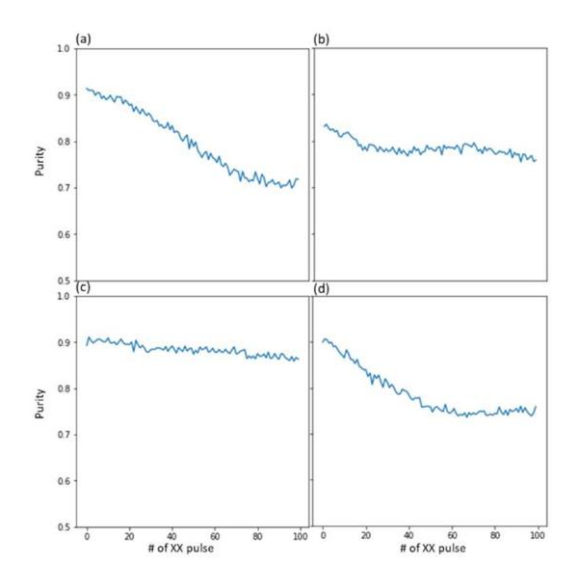


Figure 4.2 Single qubit purity changes for the $(X)^2$ gate. In each subplot, the state purity as a function of the number of applied $(X)^2$ gates are plotted. (a) – (d) corresponds to the initial state = $|0\rangle$, $|1\rangle$, $|+\rangle$, $|-\rangle$, respectively. All experiments were performed on ibmq bogota.

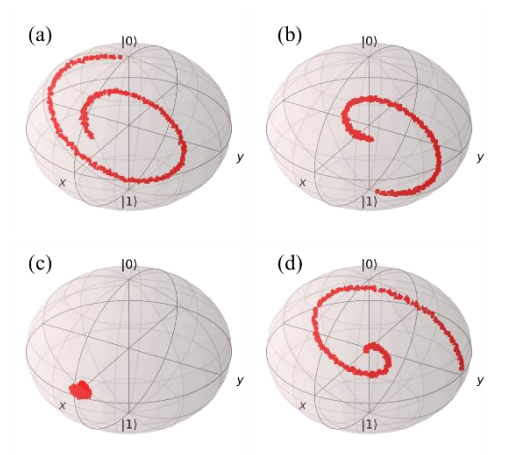


Figure 4.3 Bloch Sphere Dynamics for the $(X)^2$ Gate Sequences. We initialize the qubit in different initial states, $|0\rangle$, $|1\rangle$, $|+\rangle$, $|-\rangle$, and apply $(X)^2$ gates from $0\sim300$ times to analyze the dynamics. A dot represents the Bloch vector for the single-qubit state, and the dot is traced continuously with an increasing number of $(X)^2$ gates. (a)-(d) all show the effect of rotating around the X-axis and shortening towards the center. All experiments were performed on ibmq_bogota.

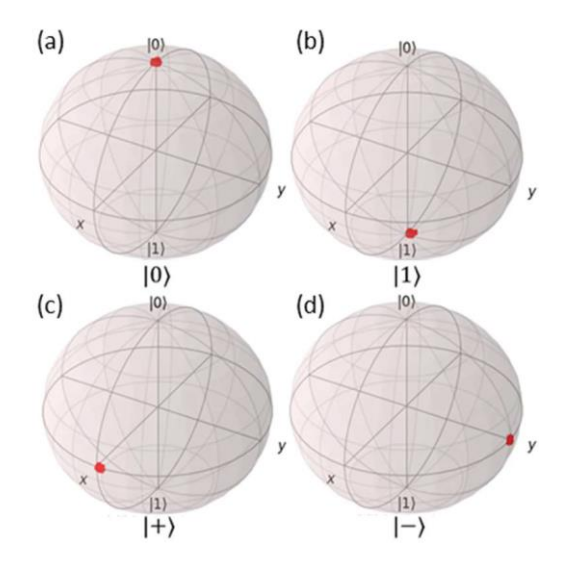


Figure 4.4 Bloch sphere dynamics for the $(Z)^2$ gate sequences. The initial states of (a), (b), (c), (d) are $|0\rangle$, $|1\rangle$, $|+\rangle$, respectively. We initialize the qubit in four basis state and apply $(Z)^2$ gates from $0\sim100$ times to analyze their behaviors. Each point on the Bloch Sphere represent the density matrix at each number of applied $(Z)^2$ gates. Experiments were performed on ibmq paris.

4.2 Noise decomposition and simulation of $(X)^2$ gates

Here we use simple mathematical models to describe the dynamics of $(X)^2$ gates. The quantum process could be seen as a combination of systematic, coherent rotation and depolarization error. In the following experiments, we thus use equation (2.5.2) to fit the dynamics obtained in Figure 4.3 and get the error rate of depolarizing error and the noise Hamiltonian of each step. We took both coherent rotation and depolarization (Table 2) into account in our model. In Figure 4.5, we plot both the Bloch sphere dynamics for the (X)² gates (green dots), and the fitted dynamics (red dots). The variable noise information suggests the state-dependent nature of the quantum gate noise and could be investigated in the future. We note that the fitting is suitable for the early steps but gets worse for long time steps; the fitting method could be improved using the CN method; however, the analyzed noise Hamiltonians are almost equal. Here we only show the result of the Forward Euler method. After collecting the Hamiltonian, we calculate the deviation and the mean of the distribution to fit the Hamiltonian distribution. In Figure 4.6, we can see that the noise distribution looks like the Lorentz distribution. After fully reproducing the open system dynamics, there are many things for us to analyze. In the current stage, we find that, unlike the assumption in section 2.6, the non-Gaussian distribution has appeared, which will have significant implications for the noise mitigation method and

the error corrections method.

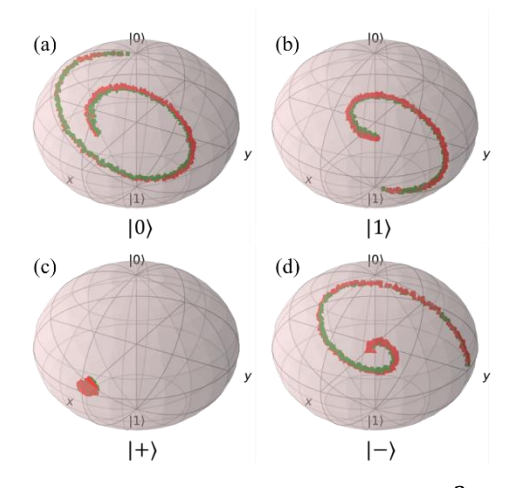


Figure 4.5 Fitting of the Bloch sphere dynamics for the $(X)^2$ gates. The Bloch sphere dynamics for $(X)^2$ gates (green) in Figure 5 are fitted with qubit dynamics with noise Hamiltonian and depolarizing channel.

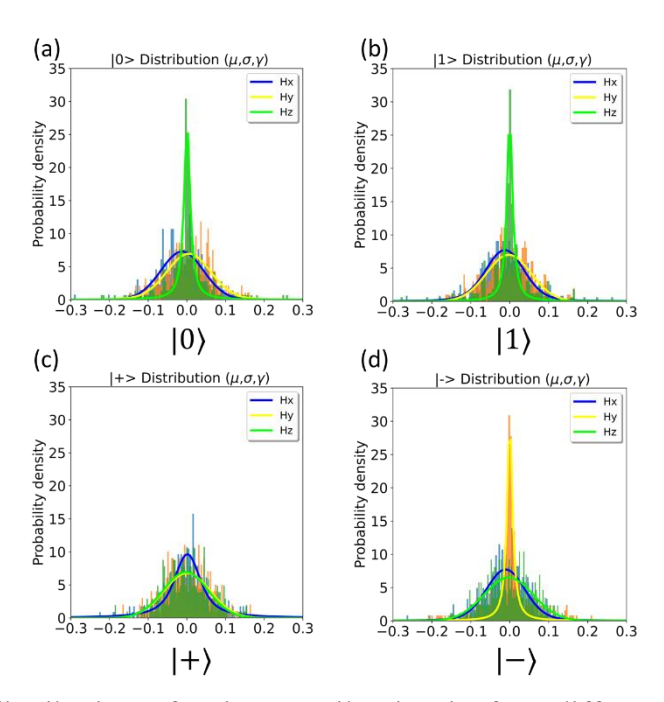


Figure 4.6 The distribution of noise Hamiltonian in four different initial states. By applying the analysis method mentioned in Appendix A, we can get the Hamiltonian of each step. We can see that only when the initial state is $|+\rangle$, the H_z noise distribution has more Gaussianity, while the H_z noise distributions in other initial states show highly

non-Gaussianity.

4.3 Correlation error in a two-qubit system

We designed two circuits to check whether there is a correlation between two independent systems (not entangled qubits) (**Figure 4.7**). In an experiment (a), only qubit q_0 has been applied the $(X)^2$ gates. And in experiment (b), both qubit q_0 and qubit q_1 has been applied the $(X)^2$ gates. Even the gate is imperfect, the Bloch sphere dynamics of (a) and (b) should be the same since the two systems are not entangled. However, in **Figure 4.8**, the trajectories on the Bloch sphere have different behavior. We have observed the correlated noises when applying X^2 gates on the neighbor qubit.

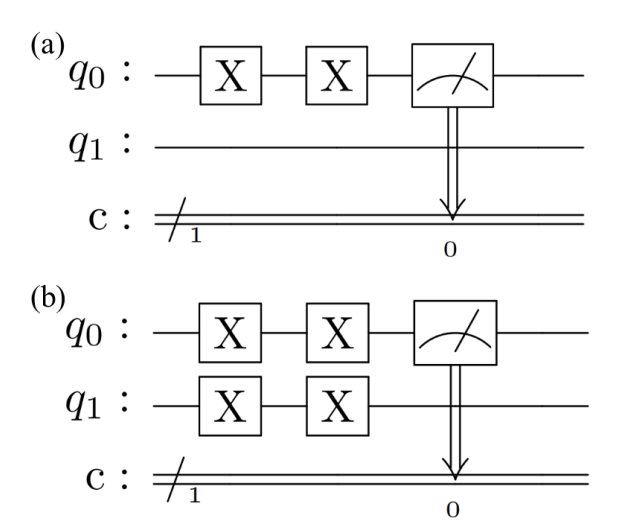


Figure 4.7 The designed circuits for observing the correlation between two qubits. The initial states preparations and the increasing number of $(X)^2$ gates have not shown in this figure. We initialize the qubit in four basis state and apply $(X)^2$ gates from $0\sim150$ times to analyze their behaviors. We should notice that two qubits are not entangled in (a) and (b).

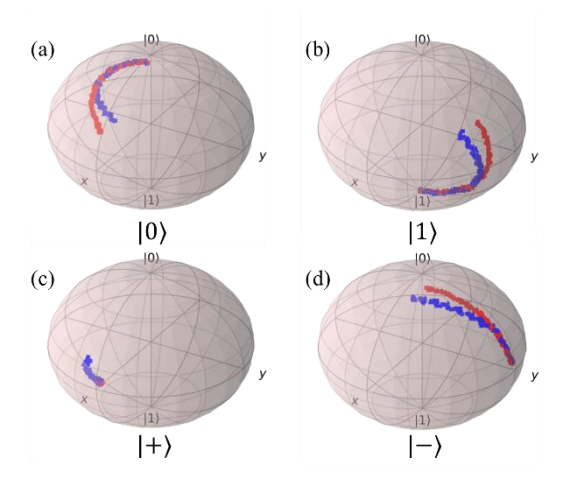


Figure 4.8 The designed circuits for observing the correlation between two qubits. The qubit q_1 in red trajectory has not been applied the $(X)^2$ gates while in blue trajectory q_1 has been applied the $(X)^2$. Even two qubits are not entangled, and the measurement is only applied to the qubit q_0 , the gates applied on qubit q_1 show effect on qubit q_0 . Experiments were performed on ibmq_paris.

4.4 Compensating pulse sequence design –(XZXZZ)² gates

As mentioned earlier, we found that there is no error in $(Z)^2$ gates on the Bloch sphere (**Figure 4.4**). Therefore, we employ the method of dynamical decoupling. To eliminate the rotation error, we choose a spin-echo type sequence $(XZ)^2$. **Figure 4.9** is a projection of the Bloch sphere. First, we hit an X, it will over-rotate, then we apply a phase gate to flip, and another X will compensate for the over-rotation angle. Finally, we apply a phase gate again to form an identity. To pursue higher stability, we choose the second-order term $(XZXZZ)^2$. In **Figure 4.10**, we can see that the designed gate sequences successfully eliminate the rotation error and leave only depolarizing error.

We can view (XZXZZ)² gates as the decoherence-inducing gates, the number of

gates is controllable, which means we can determine the amount of introduced noises.

This specific gate sequence can be used to introduce the specific noises when simulating the open quantum system.¹⁶

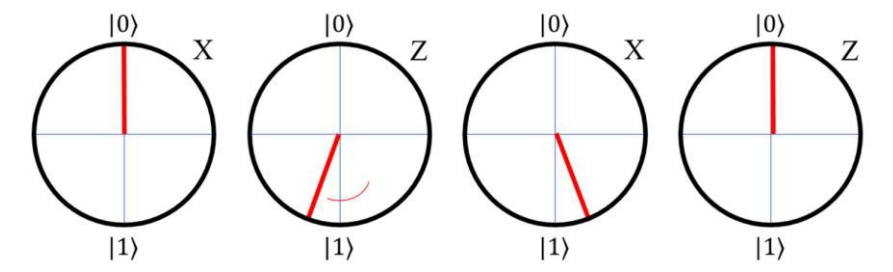


Figure 4.9 Illustration of the compensating pulse sequences design. The circle is a projection of the Bloch sphere on the YZ plane. To dynamically correct the over-rotation error, first, a X gate is applied. The over-rotation is then turned into an under-rotation by applying a phase (Z) gate. The over-rotation of the second applying X gates then cancels the under-rotation. Finally, another Z gate is applied to recover identity.

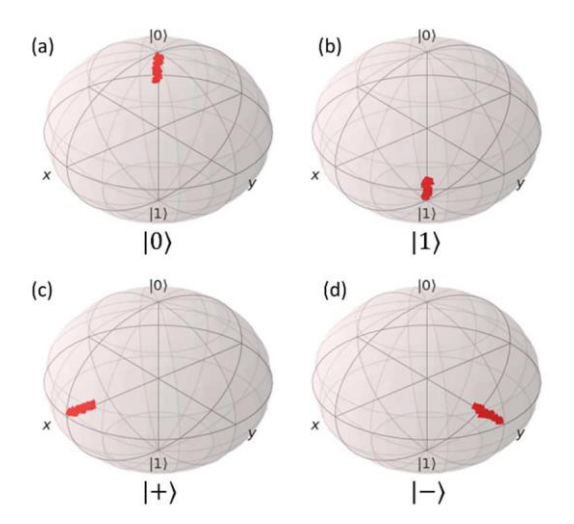


Figure 4.10 Bloch sphere Dynamics for the $(XZXZZ)^2$ gates. We initialize the qubit in four initial states and apply $(XZXZZ)^2$ gates from $0\sim100$ times to analyze their behaviors. Each point on the Bloch Sphere represent the density matrix at each number of applied $(XZXZZ)^2$ gates. Experiments were performed on ibmq_manhattan.

5 Conclusion

Quantum Error Correction is the most important step for the ultimate universal faulttolerant quantum computer, but they rely on a certain assumption of the noise. A better
comprehension of the noises would benefit analyzing the performance of the quantum
computer. We provide a procedure to analyze noise composition for each possible
quantum dynamic. We utilize the known noise channel and the quantum master equation
to decompose the noise and obtain the error rates and noise Hamiltonian in each
experiment step. After obtaining the information about noises in the experiment, we can
reproduce the Bloch sphere dynamic. That is, we can extract the information of noise in
the experiment. We can study how noises from the environment affect the system and
how noises change over time.

We can get a deeper understanding of noise by analyzing the dynamics of Hamiltonian and error rate. We reveal that the imperfection of $(X)^2$ consists of over-rotation errors from gate error and decoherent errors from the environment. However, the conventional benchmark protocol only yields the average gate fidelity for the calibration of gate performance, which would provide limited information to describe the composition of the gate noises properly. What's more, we find that the non-Gaussian distribution and

correlated noises have appeared, which have significant implications for the noise mitigation method and the error corrections method. This algorithm help us better understand noise and its behavior of noise. Besides, the result excites the concept of utilizing the noise. We design hardware-specific gate sequences to mitigate or transform a certain type of quantum noise. With designed gate sequences, we can generate a certain type of noise for better performance for quantum simulation, error mitigation, and quantum error correction. For example, if we design the gates that cause markovian noises, they can be applied to simulate the noises in the open quantum systems.

6 References

- 1. Feynman, R. P., Simulating physics with computers. *International Journal of Theoretical Physics* **1982**, *21* (6), 467-488.
- 2. Shor, P. W. In *Algorithms for quantum computation: discrete logarithms and factoring*, Proceedings 35th Annual Symposium on Foundations of Computer Science, 20-22 Nov. 1994; 1994; pp 124-134.
- 3. Boixo, S.; Isakov, S. V.; Smelyanskiy, V. N.; Babbush, R.; Ding, N.; Jiang, Z.; Bremner, M. J.; Martinis, J. M.; Neven, H., Characterizing quantum supremacy in near-term devices. *Nature Physics* **2018**, *14* (6), 595-600.
- 4. Buchanan, W.; Woodward, A., Will quantum computers be the end of public key encryption? *Journal of Cyber Security Technology* **2017**, *I* (1), 1-22.
- Biamonte, J.; Wittek, P.; Pancotti, N.; Rebentrost, P.; Wiebe, N.; Lloyd,
 S., Quantum machine learning. *Nature* 2017, 549 (7671), 195-202.
- 6. Georgescu, I. M.; Ashhab, S.; Nori, F., Quantum simulation. *Reviews of Modern Physics* **2014**, *86* (1), 153-185.
- 7. Cody Jones, N.; Whitfield, J. D.; McMahon, P. L.; Yung, M.-H.; Meter, R. V.; Aspuru-Guzik, A.; Yamamoto, Y., Faster quantum chemistry simulation on fault-tolerant quantum computers. *New Journal of Physics* **2012**, *14* (11), 115023.

- 8. "Randomized Benchmarking" *Qiskit.org*, https://qiskit.org/textbook/ch-quantum-hardware/randomized-benchmarking.html.
- 9. M. A. Nielsen and I. Chuang, *Quantum computation and quantum information*. 2002; p381-426.
- 10. "Pauli measurements Azure Quantum" *Microsoft Docs*, 1 Feb. 2021, https://docs.microsoft.com/zh-tw/azure/quantum/concepts-pauli-measurements.
 - 11. H. Breuer, and F. Petruccione, The theory of open quantum systems. 2002;
- 12. R. Kubo, "Stochastic liouville equations", *J. Math. Phys.*, vol. 4, no. 2, pp. 174-183, 1963.
- 13. Cheng, Y. C.; Silbey, R. J., Stochastic Liouville equation approach for the effect of noise in quantum computations. *Physical Review A* **2004**, *69* (5), 052325.
- Fischer, Hans. "A history of the central limit theorem" (PDF). Springer New York Dordrecht Heidelberg London. Retrieved 29 April 2021.
- 15. Butcher, John C. (2003), Numerical Methods for Ordinary Differential Equations, New York: John Wiley & Sons, ISBN 978-0-471-96758-3.
- 16 Shin Sun; Li-Chai Shi; Yuan-Chung Cheng; Efficient Quantum Simulation of Open Quantum System Dynamics on Noisy Quantum Computers. https://arxiv.org/abs/2106.12882

7 Appendix

Appendix A. Mathematical details in the Forward Euler method

To describe an open quantum system, we can use the quantum master equation:

$$\frac{d\rho(t)}{dt} = -\frac{i}{\hbar}[H(t), \rho(t)] + p\sum_{i} \left(L_{i}\rho(t)L_{i}^{\dagger} - \frac{1}{2}\left\{L_{i}^{\dagger}L_{i}\rho(t)\right\}\right), \quad (A.1)$$

where H is noise Hamiltonian, which causes the X gate to be over-rotating, p is the error rate and L_i corresponds to error operators. With density matrixes obtained from the experiment, we need to solve the equation to thoroughly understand this quantum dynamics system by finding the noise Hamiltonian and error rate of the quantum dynamics.

Assuming that the point we measure is dense enough, we discretize the equation and write the equation (To simplify the equation, we used $R[\rho]$ to represent $p\sum_i \left(L_i\rho(t)L_i^{\dagger}-\frac{1}{2}\{L_i^{\dagger}L_i\rho(t)\}\right)$):

$$\frac{\rho(t_{n+1}) - \rho(t_n)}{\Delta t} = -i[H(t_n), \rho(t_n)] + R[\rho(t_n)], \tag{A.2}$$

where n is the n^{th} measurement density matrix that corresponds to the number of $(X)^2$ gates. And the fitting density matrix of the next step is:

$$\rho_{fit}(t_{n+1}) = \rho(t_n) - \Delta t(i[H(t_n), \rho(t_n)] + R[\rho(t_n)]). \tag{A.3}$$

To solve the equation, we first present $H(t_n)$ and $\rho(t_n)$ as:

$$\rho(t_n) = \frac{1 + r_x(t_n)\sigma_X + r_y(t_n)\sigma_Y + r_z(t_n)\sigma_Z}{2},$$
(A.4)

where $\sigma_{X,Y,Z}$ is Pauli matrix.

$$H(t_n) = H_x(t_n)\sigma_X + H_Y(t_n)\sigma_Y + H_Z(t_n)\sigma_Z. \tag{A.5}$$

The desired value of equation (A.3) is p and $H(t_n)$ or $H_x(t_n)$ $H_y(t_n)$ and $H_z(t_n)$.

Because we only consider the one qubit system, we first set the error rate p=0 and assume that

$$\frac{\rho(t_{n+1}) - \rho(t_n)}{\Delta t} = \begin{pmatrix} b_1 & b_2 - b_3 i \\ b_2 + b_3 i & b_1 \end{pmatrix}, \tag{A.6}$$

while

$$-i[H(t_n), \rho(t_n)] = \begin{pmatrix} b_1 & b_2 - b_3 i \\ b_2 + b_3 i & b_1 \end{pmatrix}.$$
 (A.7)

We can use equations (A.4) and (A.5) to extend $-i[H(t_n), \rho(t_n)]$ and get

$$-i[H(t_n), \rho(t_n)] = -i\{H(t_n)\rho(t_n) - \rho(t_n)H(t_n)\}$$

$$= \begin{pmatrix} (H_x r_y - H_y r_x) & (H_y r_z - H_z r_y) - i(H_z r_x - H_x r_z) \\ (H_y r_z - H_z r_y) + i(H_z r_x - H_x r_z) & (H_x r_y - H_y r_x) \end{pmatrix},$$
(A.8)

In contrast to the element in equations (A.7) and (A.8), we know that

$$\begin{pmatrix} r_y & -r_x & 0\\ 0 & r_z & -r_y\\ -r_z & 0 & r_x \end{pmatrix} = A \tag{A.9}$$

$$A \cdot \begin{pmatrix} H_x \\ H_y \\ H_z \end{pmatrix} = \begin{pmatrix} r_y & -r_x & 0 \\ 0 & r_z & -r_y \\ -r_z & 0 & r_x \end{pmatrix} \cdot \begin{pmatrix} H_x \\ H_y \\ H_z \end{pmatrix} = \begin{pmatrix} b_1 \\ b_2 \\ b_3 \end{pmatrix}. \tag{A.10}$$

We can get the Hamiltonian H by using A^{-1} :

$$\begin{pmatrix} H_x \\ H_y \\ H_z \end{pmatrix} = A^{-1} \cdot \begin{pmatrix} b_1 \\ b_2 \\ b_3 \end{pmatrix}, \tag{A.11}$$

where A⁻¹ is Pseudo Inverse Matrix. (A generalization of the inverse matrix when

the matrix is singular) Because we know the density matrix of each step, so after we get the Hamiltonian $H(t_n)$, we can find out the most appropriate error rate p by minimizing the trace distance between $\rho(t_{n+1})$ and $\rho_{fit}(t_{n+1})$ in equation (A.2).

$$T(\rho, \rho_{fit}) = ||\rho(t_{n+1}) - \rho_{fit}(t_{n+1})||/2$$
(A.11)

Appendix B. Application details in the Crank-Nicolson method

For a (X)² Bloch sphere dynamics (**Figure B.1**), we draw the vector length change in each step (**Figure B.2**). We can use a linear equation to fit the dynamics of vector length, which means that we can use only the initial value of the vector length to know the overall depolarizing effect. The linear equation can be written as

$$y(t_n) = ax(t_n) + b, (B.1)$$

Where a corresponds to the depolarizing effect and b corresponds to the initial measurement error.

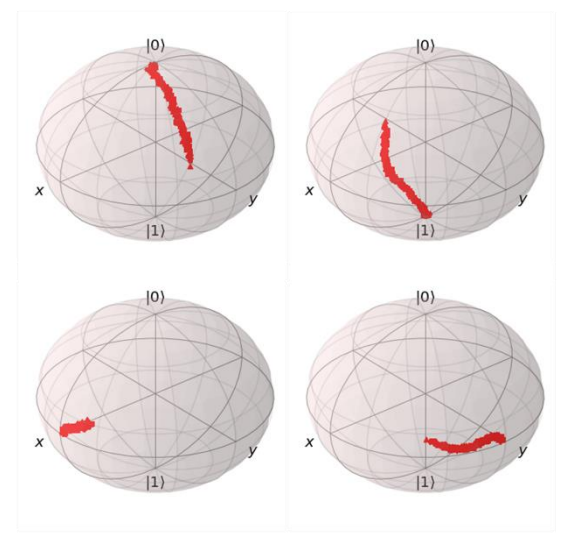


Figure B.1 Bloch sphere Dynamics for the $(X)^2$ gates. We initialize the qubit in four initial states and apply $(X)^2$ gates from $0\sim300$ times to analyze their behaviors. Experiments were performed on ibmq paris.

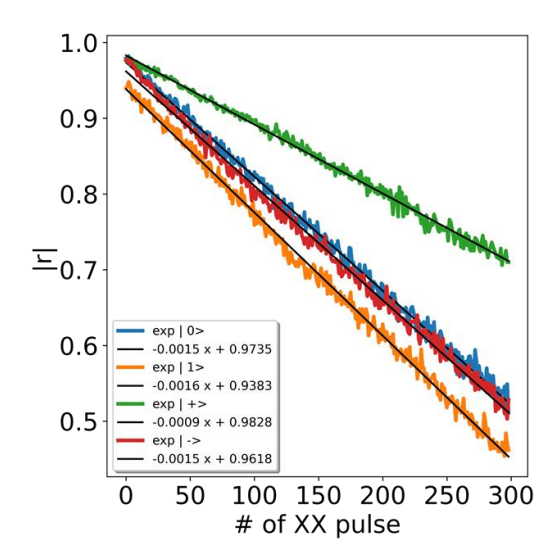


Figure B.2 Change of vector length at each step. We draw the change of vector length in Figure B.1 and finds that the correlation is linear (0th order).

With these properties, we can first normalize the Bloch vector from the experiment, search the best Hamiltonian with minimum trace distance mentioned in equation (A.11), and use the theory vector length value from the linear curve to rescale the vector length. We must use the Crank-Nicolson method to unitary propagate the system as the equation:

$$\frac{\rho(t_{n+1}) - \rho(t_n)}{\Delta t} = \frac{1}{2} \left(-i[H(t_n), \rho(t_n)] - i[H(t_n), \rho(t_{n+1})] \right), \quad (B.2)$$

By this method, we can share that the Hamiltonian information only represents the rotation noises from imperfect gates. In the Forward Euler method, Hamiltonian information might include the depolarizing noises that make the vector short. We draw

the trace distance at each step in different initial states to compare the two methods. We can find that the Crank-Nicolson method (black lines) has a smaller trace distance than the Forward Euler method (colored lines). In other words, the Crank-Nicolson method performs better in simulating the Bloch sphere dynamics.

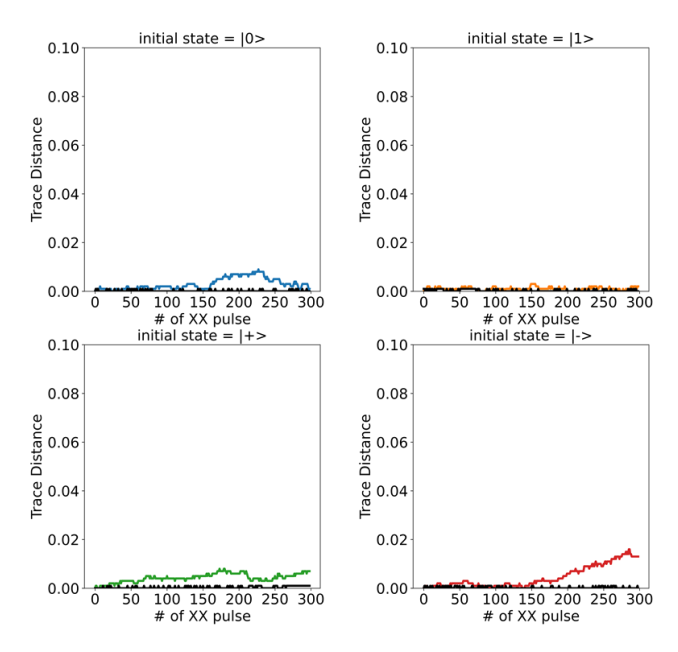


Figure B.2 Trace distance of different methods in different initial states. The black lines represent the results from the Crank-Nicolson method, while the colored lines represent the results from the Forward Euler method.

Appendix C. Variance of the depolarizing rate of $(XZXZZ)^2$ and $(X)^2$

To discuss the variation of the decoherence noises in Bloch sphere dynamics under $(XZXZZ)^2$ and $(X)^2$ gates, and fit the dynamics with our model. Three consecutive experiments were done and fit independently to support statistical analysis. We then extract the depolarization rate to assess their difference across devices and days (), which could provide information about the amount of random noises introduced by the gate sequences. For the $(XZXZZ)^2$ case, the depolarization rate shows a systematic trend across devices (Fastest: Manhattan, Slowest: Bogota). In the case of manhattan, the

depolarization rate exhibited large fluctuations and was not significantly different across days. In the case of paris and bogota, the deviation of noises was much smaller, suggesting the stability of the noises under $(XZXZZ)^2$ were better than manhattan. Except on 12/27, the depolarization rates on three devices were all quantitively different from others. As for the case of $(X)^2$ gates, the depolarization rates were all lower than that of $(XZXZZ)^2$ due to a smaller number of pulses per identity, the stabilities were also better in general.

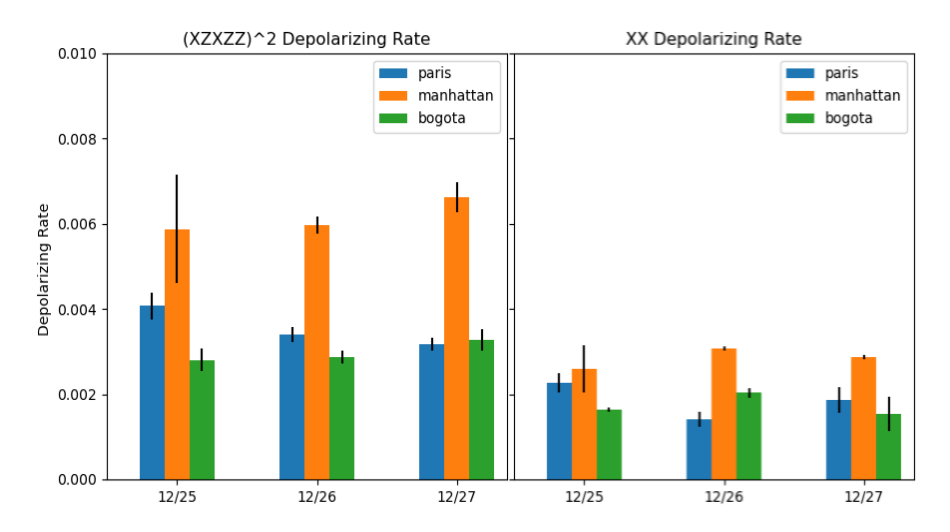


Figure C.1 Depolarization rates of $(XZXZZ)^2$ and $(X)^2$ on different devices and time.